Cooperative-Motion-Induced Structural Evolution in Dusty-Plasma Liquids with Microheterogeneity: Rupture, Rotation, Healing, and Growth of Ordered Domains

Chi Yang, Chong-Wai Io, and Lin I

Department of Physics and Center for Complex Systems, National Central University, Jhongli, Taiwan 32001, Republic of China

(Received 27 June 2012; published 26 November 2012)

The cooperative motion induced structural evolution of the liquid with microheterogeneity is investigated in quasi-2D dusty plasma liquids, through direct optical visualization. A novel bond-dynamics analysis is used to further classify the robust cooperative 2D clusters into static, rotating, and drifting patches, beyond the earlier findings of the cooperative hopping strings and bands. The relative motion between two adjacent clusters causes the formation of a fractal network with narrow shear strips along the cluster interface. The rotation of the large ordered patch through rupturing into multiple rotating patches followed by the healing process, and the growth to a larger ordered patch by aligning the different lattice orientations of the adjacent ordered domains through patch rupturing, rotation, drifting, and merging are the key processes for the microstructural evolution.

DOI: 10.1103/PhysRevLett.109.225003 PACS numbers: 52.27.Lw, 61.20.-p, 64.70.pm

Microscopically, unlike intuitive expectation, cold or glass-forming liquid is not completely disordered [1–10]. Under solidlike dense packing, the competition between the correlation generated by the strong interaction and the disorder by the weak thermal agitation leads to heterogeneities in structure and motion, which affect the physical properties of the cooled liquid [1–10]. Spatially, various sized crystalline ordered domains (CODs) coexist with defect clusters around COD interfaces [1–5]. Temporally, particles alternately exhibit small amplitude thermal oscillations (cage rattling) in caging wells formed by their nearest neighbors, and cooperative hopping (cage jumping) over caging barriers after accumulating sufficient constructive perturbations [1–4,6–10]. It in turn causes structural rearrangement (SR).

Macroscopically, liquids are treated as incompressible continuous media exhibiting smooth plastic deformation under shear stress. Vortical, drifting and shear motions are the basic cooperative motions under perturbation [11]. Down to the discrete level, in the cold liquid, the solidlike CODs are harder to deform plastically. Regions around poorly interlocked defect clusters are more vulnerable to thermal kicks [12], and easier to initiate hopping or COD rupture. It is interesting to find the basic thermal induced cooperative excitations at the microscopic level, and how they affect SR.

The previous numerical and experimental studies indicated that hopping occurs cooperatively in the forms of stringlike and bandlike clusters, but without further detailed classification [1,2,6–9]. For SR, Stillinger proposed that the liquid is composed of strongly bonded domains separated by the irregular wall with weakened bonds, and undergoes SR with *tearing* and *repairing* around the irregular domain walls [13]; but without experimental evidence. The more detailed classification of basic cooperative excitations, basic dynamical processes of SR, and how they are correlated to affect the dynamical evolutions of microstructure and motion, are still elusive fundamental issues. These issues are difficult to address by the commonly used information of single-particle motion and bond breaking [10], but without more detailed information of relative particle motion. In this Letter, for the first time, the above issues are experimentally investigated in the quasi-2D dusty plasma liquids (DPLs) with structural and dynamical heterogeneities. The novel method of bond-dynamics analysis, based on the information from the variations of the length, the angle, and the position of the bond connecting adjacent particles, is applied for investigation.

The DPL can be formed by micrometer sized particles suspended in the low pressure rf discharge [2,14–19], through the screened Coulomb interaction due to strong negative charging ($\sim 10^4$ e/particle) on particles. It is a good platform to understand the generic behaviors of the Yukawa liquid at the microscopic level under different thermal agitation and external stresses through direct particle motion tracking [2,14–23].

The experiment is conducted in a cylindrical symmetric rf dusty plasma system [24], as described elsewhere [23]. A hollow coaxial cylindrical trap with 4.1 cm inner diameter, and 14 mm height is put on the bottom electrode, in which the DPL formed by polystyrene particles (7 ± 0.4 μm in diameter) are confined by the sheath field adjacent to the trap wall. The weakly ionized glow discharge ($n_e \sim 10^9$ cm^{-3}) is generated in 250 mTorr Ar gas using a 14 MHz rf power system. The estimated Debye length and the charges on the particles are in the order of 10^{-1} mm and a few to ten thousand e/particle, respectively. The wake field effect of the downward ion wind lines up particles into stiff vertical short chains [25], with about 14 particles in each chain. Particles along the same chain move together horizontally, without vertical particle

flipping. It makes the system a good quasi-2D system. The interchain distance a is about 0.3 mm. The particle images illuminated by a thin laser sheet are recorded at 30 Hz sampling rate by a CCD through a microscope. The steady hot run II at 2.2 W, and the cold run I at 1.6 W are used for the study.

Figures 1(a) and 1(e) show the plots of 7 s particle trajectories for runs I and II, respectively. The background gray grids indicate the initial positions of particles and the bonds connecting adjacent particles. CODs with a triangular lattice structure coexist with surrounding defect clusters of sevenfold and fivefold defects. Figure 2(a) depicts the spatial correlation function, $g_{6r} = \langle \Psi_6^*(0)\Psi_6(r)\rangle$, of the bond-orientational order Ψ_6 [26]. Cooling leads to longer correlation length of g_{6r} (under the emergence of large CODs up to 10–15 a in width), slower motion, and slower SR. The time scale, τ_6, for the temporal correlation function $g_{6\tau} = \langle \Psi_6^*(t+\tau)\Psi_6(t)\rangle$ decays to e^{-1} through SR is about 2.4 and 7 s for the hot run II and the cold run I, respectively [24].

Let us focus on the cold run I [Fig. 1(a)]. At first glance, particle motion can be roughly divided into two types: cage rattling with small displacement, and hopping with large displacement. They occur in the form of clusters as 2D patches or 1D strings with various sizes and shapes as reported in previous studies [2,8]. Cooling reduces (increases) the fraction of the stringlike (bandlike) hopping. In addition to the single-particle displacement, the changes of the length and the angle of the bond between two neighboring particles, δd and $\delta\theta$ respectively, over 7 s are used as indicators for classifying cooperative motion [Figs. 1(b), 1(c), 1(f), and 1(g)] [27]. Distinct patches (domains) separated by narrow strips can be observed.

Using $|\delta d| < 0.2\ a$ in 7 s as a criteria, the robust cooperative clusters temporarily sustaining their microstructure in 7 s can be sorted out [e.g., see the patch with small $|\delta d|$ in Fig. 1(c)]. With information regarding whether $\delta\theta > (<) 0.1$ rad and δR (the displacement of the center of mass of the cluster) $> (<0.2)\ a$, they can be classified into the following four types: (A) static patches dominated by cage rattling, (B) drifting patches, (C) rotating patches, and (D) 1D hopping strings, as shown in the circled regions in Fig. 1(a). Types A and C are the dominate excitations.

The relative shear between two adjacent robust clusters leads to a type E excitation, the narrow strip 1 a in width with strong shear along the cluster interface, as indicated by the narrow strips in the $\delta\theta$ plot [Fig. 1(c)]. The stringlike type D excitation induces two parallel shear strips with opposite shear directions. All the bonds in the shear strip rotate along the same direction with a similar large $\delta\theta$. It induces alternate stretching (with possible bond breaking) and compression of the transverse bonds in the shear strip (see the alternate colors of the δd plot, [Fig. 1(b)]. The strong bond elongation in the shear strip causes subsequent patch rupture and healing with bond breaking and reconnection. It can be viewed as the propagation (along the shear strip) of the dislocation defect initially located at or inside the patch boundary, where the microstructure is more vulnerable to thermal agitation [19,21]. The shear strips with various lengths form a time varying fractal network as shown in Figs. 1(c) and 3 and S2 of [24]. The fractal (correlation) dimension is measured from the exponent of the double logarithmic plot of the averaged number of bonds (N_s) of the shear strip in the circle centered at each bond in the shear strip, with increasing radius r [Fig. 2(b)] [28]. The fractal dimensions are 1.61 and 1.95 for runs I and II, respectively.

Figure 2(c) further depicts the fractions of bonds involving in types A to E excitations for the two runs. The stronger correlation at lower temperature makes 2D patch-type excitations dominate in the cold run. Increasing temperature increases thermal agitation, reduces the

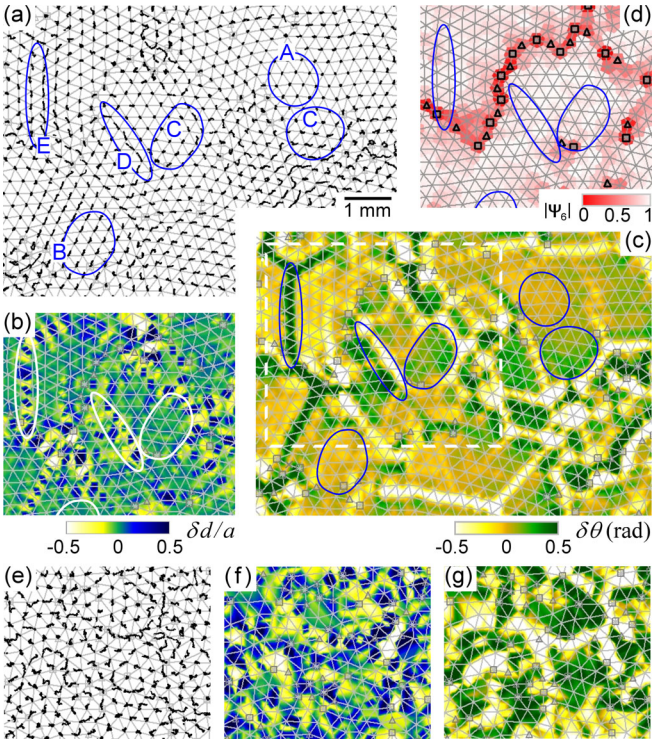

FIG. 1 (color online). (a)–(c) The plots of the particle trajectory, the bond-length variation δd, and the bond-angle variation $\delta\theta$ in 7 s intervals for the cold run I. The background triangulated grids show the initial particle configuration of the 7 s interval. The squares and the triangles correspond to the sevenfold and fivefold defects respectively. The regions $\delta\theta > (<0)$ correspond to the patches or bonds in the narrow shear strip with counterclockwise (clockwise) rotations. The circled region shows the examples of different types of cooperative motions. (d) The corresponding $|\Psi_6|$ plot for the cold run I. (b) and (d) are from the region in the dashed rectangle of (c). (e) to (g), the plots of particle trajectories, δd, $\delta\theta$, respectively, in the 7 s interval for the hot run II.

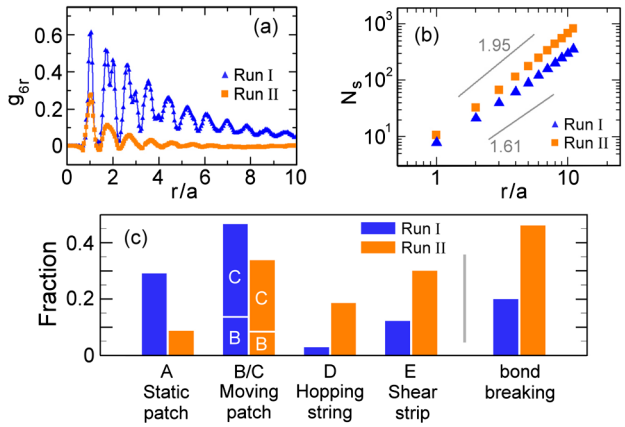

FIG. 2 (color online). (a) The spatial correlation of Ψ_6, g_{6r}, versus r for both runs. (b) The averaged numbers of bonds (N_s) of shear strips in circles centered at bonds in shear strips versus circle radius r for runs I and II. The numbers by the gray lines correspond to the fractal dimensions of the skeletons of shear strips. (c) The fraction of bonds participating in different types of cooperative motions for both runs. B and C represent drifting and rotating patches, respectively.

averaged sizes and the fraction of 2D patches, and increases the fractions of 1D excitations (hopping strings and shear strips) and breaking bonds [Figs. 1(e), 1(g), and 2(c)]. The shorter and less straight shear strips also make their fractal structure more 2D like.

Now let us focus on the dynamics of cooperative excitations and SRs for run I. Figure 1(c) and Fig. S2 in the Supplemental Material [24] show that the cold liquid can be viewed as a patchwork composed of many interacting and evolving patches, as proposed by Stillinger [13]. Intuitively, the strong particle interlocking makes CODs more solidlike and harder to deform plastically. They have a greater tendency to sustain their microstructure and exhibit cooperative rotation or drift, under weak thermal kicks. However, they are not unbreakable. The basic processes leading to SR, which change their shapes, sizes, and orientations are identified and discussed below.

The sequential plots of $\delta\theta$ with the 7 s interval of Figs. 3(a) to 3(d) with the initial microstructure in each plot give typical examples. The arrows indicate the rotation directions of the patches. From the lattice orientations in Figs. 3(c) and 3(d), we can see that the center large COD rotates clockwise. Figure 3(c) shows that five clockwise rotating yellow patches are excited in the left region. It causes the clockwise rotation of lattice lines (e.g., lines L3 and L4) with the strong kinks at the shear strip. Rotation stops and the ruptured patches are healed back to a large COD through lattice-line reconnection [see the dashed bonds in Fig. 3(d)]. Namely, the large-COD rotation can be achieved by rupture along the shear strips into smaller patches with the same rotating direction and then healing to the large COD. Similar processes move to other regions [see the different rotating patches in other region of Fig. 3(d)] later.

Figure 3(a) (right part) shows an example of another excitation with six clockwise rotating patches sharing the same center vertex, and separated by six shear strips. After the excitation, the region with defects and diverging lattice lines indicated by L1 and L2 from left to right is healed to the defect-free crystalline structure [see the right region of Fig. 3(b)].

What is the physical origin for the above process? The persistent rotation of a large COD with irregular shape is difficult, because of the large strain energy induced under the large relative particle displacement around the COD boundary, especially around its long ends. It is cheaper to be ruptured into smaller patches rotating around their own centers with the same rotating direction, and then merge to a large patch with reconnected and rotated lattice lines. Dissociation and merging of vortices also occur in

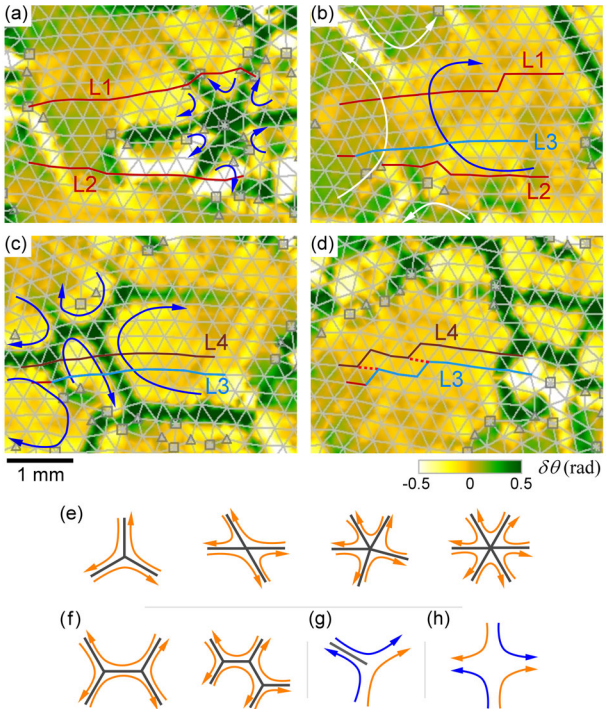

FIG. 3 (color online). (a) to (d) The sequential plots with 7 s separation showing structural evolution, associated with the excitations of multiple rotating patches. The color (gray level) reflects $\delta\theta$ in 7 s. The arrows indicate the rotating direction. The triangulated grids show the initial particle configuration of each time interval. Patch rupturing, rotating, and healing (causing the labeled lattice line breaking and reconnection) are the basic processes for SR. (e) to (g) The sketches showing the few commonly observed basic cooperative excitations with multiple rotating patches (with directions indicated by arrows), separated by shear strips (indicated by the straight edges). (h) The hardly occurring excitation of rotating patches with alternate rotation directions.

macroscopic turbulent flows [12]. However, the lifetime of the microscopic vortical excitation in the cooled liquid is much shorter due to the strong dissipation through interaction with surrounding patches. The strain energy is released and rotation stops after bond breaking and reconnection. It makes cooperative excitations last only a few seconds in a stick-slip way (see the evolutions of the $\delta\theta$ contour plots in Figs. 3 and 4).

The sketches in Fig. 3(e) show the few observed basic excitations of multiple patches with the same rotating direction (indicated by the curves with arrow heads), which cause the formation of the single vertexes connected to three to six edges (shear strips), represented by the gray thick lines. The one with three edges is the most commonly observed excitation. Figure 3(f) shows the examples of the higher order excitations with connected three-edge excitations. The single vertexes with 5 and 6 edges usually occur in the disordered region. The single-edge excitation [Fig. 3(g)], with one patch rotating oppositely to the remaining two patches, also exists. The example of the excitation in the upper left region of Fig. 3(b) shows that the opposite rotations of the adjacent two lower patches only cause the upward bending of the horizontal lattice lines [e.g., L3 in Figs. 3(b) and 3(c)], which stops the rotation due to the large strain energy. The bent lattice lines are then tilted and straightened after the clockwise rotational excitations in Fig. 3(c). Unlike in the macroscopic fluid, the excitation in Fig. 3(h) with opposite rotation of adjacent patches occurs and persists more difficultly, because the bending of the lattice lines transverse to the particle motion direction causes too much strain energy. The few plots of Fig. S2 [24] give further examples of the different combinations of the above basic cooperative rotational excitations at different times.

The COD not only ruptures and heals, it also grows. How does a large COD form through the competition of the adjacent CODs which have different lattice orientations? Figure 4 gives a good example. The two adjacent patches [in the center and upper left regions of Fig. 4(a)] with irregular shapes and separated by stringlike defect clusters cannot align their different lattice orientations merely through the relative rotation of the large CODs, due to the large induced strain energy and bond-breaking energy cost, similar to that mentioned earlier. From 0 to 7 s, Fig. 4(d) shows the clockwise rotation of the upper left COD, through the excitation of three clockwise rotating patches. The excitation of many small counterclockwise rotating patches in the middle COD, accompanied with the upward drifting patch [see the inset with particle trajectories of Fig. 4(a)] in the lower region, can also be found in Fig. 4(d). It generates a dense cluster of defects and disrupts the middle COD [Fig. 4(b)]. After SR with further patch rupturing, rotation, and healing from 7 to 14 s [Fig. 4(e)], the lattice lines are aligned and a large COD from the left to the right is formed [Fig. 4(c)]. Namely, the growth to a large COD can be achieved by disruption, rotation, drifting, and healing of the adjacent competing large CODs.

In conclusion, we experimentally investigate the fundamental processes of cooperative micromotions, and how they affect SR dynamics in cold quasi-2D dusty plasma liquids with CODs, through the novel bond-dynamics analysis. The important findings are listed as follows. (i) Under the competition of the strong interaction and thermal agitation, the system can be viewed as a patchwork composed of interacting and evolving clusters with different cooperative motions. (ii) The cooperative clusters can be classified into 1D hopping string; and 2D static, rotating, and drifting patches. The strong shear along the cluster interface causes the observed fractal skeleton of narrow shear strips one a in width and with various lengths. (iii) The persistent rotation or drifting of a large COD is hard to achieve due to the large strain energy cost under the strong coupling among CODs. Rupturing into multiple patches with the same rotating direction, followed by healing back to the large COD through the bond breaking and reconnection along the crack strip (shear strip) is the most commonly observed excitation for the large COD rotation. (iv) COD growth can be achieved by the disruption, reorientation, and merging of the adjacent CODs with different initial lattice orientations, through excitations of small-scale rotating and drifting patches. (v) Increasing temperature increases stochastic agitation and shortens the lifetimes and the sizes of the cooperative excitations.

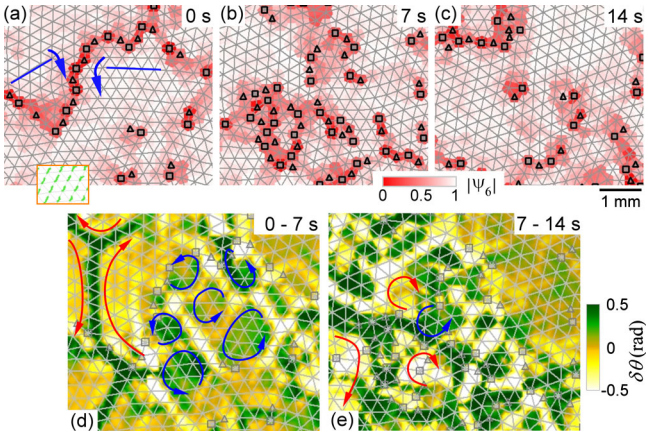

FIG. 4 (color online). The example showing the competition between CODs with different lattice orientations leading to the formation of the large COD through rupturing, rotating, drifting, and healing of CODs. (a) to (c) The sequential plots with a 7 s interval showing the structural evolution. The color (gray level) represents $|\Psi_6|$. (d) and (e) The two sequential plots showing $\delta\theta$ in 7 s intervals. The background grids indicate the initial particle configuration of each exposure. The arrows indicate the directions of patch rotation.

This work is supported by the National Science Council of the Republic of China under Contract No. NSC-99-2112-M008-002-MY3.

[1] M. M. Hurley and P. Harrowell, Phys. Rev. E **52**, 1694 (1995).
[2] Y. J. Lai and L. I, Phys. Rev. Lett. **89**, 155002 (2002); C. L. Chan, C. W. Io, and L. I, Contrib. Plasma Phys. **49**, 215 (2009), and the references therein.
[3] T. Kawasaki, T. Araki, and H. Tanaka, Phys. Rev. Lett. **99**, 215701 (2007); K. Watanabe and H. Tanaka, Phys. Rev. Lett. **100**, 158002 (2008).
[4] Y. Han, N. Y. Ha, A. M. Alsayed, and A. G. Yodh, Phys. Rev. E **77**, 041406 (2008).
[5] L. Assoud, F. Ebert, P. Keim, R. Messina, G. Maret, and H. Löwen, Phys. Rev. Lett. **102**, 238301 (2009).
[6] C. Donati, J. Douglas, W. Kob, S. Plimpton, P. Poole, and S. Glotzer, Phys. Rev. Lett. **80**, 2338 (1998).
[7] E. R. Weeks, J. C. Crocker, A. C. Levitt, A. Schofield, and D. A. Weitz, Science **287**, 627 (2000).
[8] Z. Zhang, P. J. Yunker, P. Habdas, and A. G. Yodh. Phys. Rev. Lett. **107**, 208303 (2011).
[9] R. Candelier, A. Widmer-Cooper, J. Kummerfeld, O. Dauchot, G. Biroli, P. Harrowell, and D. Reichman, Phys. Rev. Lett. **105**, 135702 (2010).
[10] R. Yamamoto and A. Onuki, J. Phys. Soc. Jpn. **66**, 2545 (1997).
[11] e.g., T. E. Faber, *Fluid Dynamics for Physicists* (Cambridge University Press, Cambridge, England, 1995).
[12] M. A. Moore and A. Perez-Garrido, Phys. Rev. Lett. **82**, 4078 (1999).
[13] F. H. Stillinger, J. Chem. Phys. **89**, 6461 (1988).
[14] e.g., G. E. Morfill and A. V. Ivlev, Rev. Mod. Phys. **81**, 1353 (2009), and the references therein.
[15] B. Liu, J. Goree, and O. S. Vaulina, Phys. Rev. Lett. **96**, 015005 (2006).
[16] Y. Feng, J. Goree, and B. Liu, Phys. Rev. Lett. **100**, 205007 (2008).
[17] P. Hartmann, A. Douglass, J. Reyes, L. Matthews, T. Hyde, A. Kovács, and Z. Donkó, Phys. Rev. Lett. **105**, 115004 (2010).
[18] K. Rypdal, B. Kozelov, S. Ratynskaia, B. Klumov, C. Knapek, and M. Rypdal, New J. Phys. **10**, 093018 (2008).
[19] C. H. Chiang and L. I, Phys. Rev. Lett. **77**, 647 (1996).
[20] V. Nosenko, S. K. Zhdanov, A. V. Ivlev, C. A. Knapek, and G. E. Morfill, Phys. Rev. Lett. **103**, 015001 (2009).
[21] V. Nosenko, S. Zhdanov, and G. E. Morfill, Phys. Rev. Lett. **99**, 025002 (2007); V. Nosenko, G. E. Morfill, and P. Rosakis, Phys. Rev. Lett. **106**, 155002 (2011).
[22] V. Nosenko, A. V. Ivlev, and G. E. Morfill, Phys. Rev. Lett. **108**, 135005 (2012).
[23] Y.-S. Su, C.-W. Io, and L. I, Phys. Rev. E **86**, 016405 (2012).
[24] See Supplemental Material at http://link.aps.org/supplemental/10.1103/PhysRevLett.109.225003 for more details about experimental system, the time scales for micromotion and structural rearrangement, and examples of particle trajectories and microstructural evolution.
[25] M. Nambu, S. V. Vladimirov, and P. K. Shukla, Phys. Lett. A **203**, 40 (1995).
[26] Ψ_6 is defined as $\Psi_6(\mathbf{r}) = (1/N)\sum_k \exp(i6\theta_k)$, where θ_k and N are the bond angle from the particle at $\mathbf{r}$ to its nearest neighbor k and the number of nearest neighbors, respectively. See K. J. Strandburg, *Bond-Orientational Order in Condensed Matter Systems* (Springer, New York, 1992).
[27] For coding the colors in the $\delta\theta$ (or δd) plots of Figs. 1, 3, and 4, the value of $\delta\theta$ (δd) of each bond is assigned at the center of each bond. Then, after the bilinear interpolation of $\delta\theta$ (δd) over the whole area are made, the contour plots of $\delta\theta$ and δd over the whole area can be made. For coding the colors in the $|\Psi_6|$ plots, the color in each Voronoi cell surrounding each particle represents the value of the corresponding $|\Psi_6|$.
[28] S. H. Strogatz, *Nonlinear Dynamics and Chaos* (Addison-Wesley, Reading, MA, 1994).